Subtracting Narrow-band Noise from LIGO Strain Data in the Third Observing Run

A. Viets[1] and M. Wade[2]

[1]*Concordia University Wisconsin, Mequon, WI 53097, USA*
[2]*Kenyon College, Gambier, OH 43022, USA*

The LIGO strain data contains narrow-band noise features due to injections from the photon calibrator and actuation system used to assist with the calibration and due to the 60 Hz AC current of the U.S. power grid, along with the accompanying harmonics of this power mains noise. These narrow-band noise features can be disruptive to searches for persistent gravitational-wave signals, such as the search for continuous wave sources and a stochastic background. In an effort to improve the data quality for these analysis efforts, the LIGO calibration team developed a method for subtracting the narrow-band photon calibrator and actuation injections and power mains noise from the strain data in LIGO's third observing run. Here we discuss the methods used to achieve this subtraction.

I. INTRODUCTION

The search for persistent gravitational waves (GWs) relies on accurate and clean measurements of the power spectral density of strain data, and such measurements are negatively impacted by the presence of narrow-band noise sources in the strain data [1]. In order to improve the data quality for persistent GW analyses, the LIGO calibration team developed and deployed a method for subtracting select sources of narrow-band noise from the LIGO strain data in LIGO-Virgo's third observing run (O3). Specifically, the developed methods focused on subtracting a few narrow-band noise sources. (1) Narrow-band injections from the photon calibrator system [2] and actuation system [3, 4], colloquially known as "calibration lines." Table I shows the calibration line frequencies present in the data and which frequencies were subtracted. (2) Narrow-band noise caused by the 60 Hz AC current of the U.S. power grid, herein known as "power mains lines." (3) Harmonics of the 60 Hz power mains lines, up to and including the 300 Hz harmonic.

The methods for subtracting the above narrow-band frequency features from LIGO strain data have been deployed in the `gstlal-calibration` software package [5]. Additional cleaning of the non-stationary 60 Hz sidebands was performed by a separate algorithm [6]. The Virgo strain data was also cleaned with both broad-band and narrow-band noise subtraction [7].

II. METHODS

Both the calibration lines and the power mains lines are tracked using auxiliary channels in the LIGO detectors, which means these noise sources have "witnesses" that can be used to determine the expected presence of the corresponding noise in the strain channel. Table II gives the channel names used as witnesses for subtracting each line enumerated in Table I.

Since there are witness channels for each line being subtracted, the subtraction can be done using the following algorithm:

1. Demodulate the strain channel and the witness channel at the appropriate frequency ω_i.

2. Compute the transfer function $T_j(\omega_i)$ between the strain channel $h(\omega_i)$ and the witness channel $w_j(\omega_i)$ at the demodulated frequency.

3. Construct a running median of the real and imaginary parts of the transfer functions. In O3, we used a 128 second running median.

4. Repeat steps (1-3) for all remaining witness channels and line frequencies.

5. Subtract the computed line noise from strain data h to produce cleaned strain data $h_{\rm clean}$:

$$h_{\rm clean} = h - \sum_i \sum_j T_j(\omega_i) w_j(\omega_i) \tag{1}$$

   where the computed line noise across all relevant frequencies is subtracted.

This algorithm can be applied in a straightforward manner to the calibration lines, but some adjustment needs to be made to accurately subtract the power mains lines. In particular, the power mains line frequencies are known to drift substantially over time (by as much as ±0.02 Hz). This is compensated for in two different ways, depending on whether latency is an issue or not.

For the high-latency calibration procedure, the low-pass filter that is used to demodulate the appropriate channels (step 1 above) can add an arbitrary latency to the overall calibration procedure without negative impact. Therefore, by using a low-pass filter that is centered in time, the changes to the power mains line frequencies are absorbed as an oscillating phase factor in the transfer functions T_j. However, in the low-latency calibration procedure, the low-pass filter cannot add latency to the process by centering it in time, as this would adversely increase the latency of calibrated data. Instead, a corrective phase factor ϕ_{corr} is included when computing the transfer function,

$$h(\omega_i) = e^{i\phi_{corr}} T(\omega_i) w(\omega_i) \tag{2}$$

where ϕ_{corr} is calculated based on the current power mains frequency, tracked using an element in the `gstlal-calibration` software package known as `lal_trackfrequency`, and the length of the low-pass filter used in demodulation.

During O3, the low-pass filter used to demodulate the signals at the frequencies of the lines being subtracted was a 20–second Blackman window applied as a finite impulse response filter. The frequency resolution of this measurement is therefore ∼0.1 Hz, so any signal present in both the strain data and the noise witness channel that is more than ∼0.1 Hz away from the frequency being subtracted will have little impact on the demodulated signal. Any signal that is present only in the strain and not in the witness channel, such as a GW signal, can also be averaged away by the 128–second running median applied to compute the transfer functions T_j. Such a signal would need to be within ∼0.01 Hz of the frequency being subtracted to impact the subtraction. Signals from transient GW events only remain in this narrow frequency band very briefly ($\lesssim$1 s), and the 128-second running median used to compute the transfer functions prevents such signals from impacting the subtraction, since a median is insensitive to any brief outliers caused by a transient signal. However, if a continuous GW signal is discovered within ∼0.01 Hz of a spectral line being subtracted using this method, its impact on the subtraction would require consideration.

III. RESULTS

Figures 1-5 show the results of subtracting the calibration lines and power mains lines from the LIGO strain data in O3 for both the L1 and H1 detectors. As can be seen in Figs. 1 and 3, the algorithm outlined in Sec. II is very effective at removing the calibration lines from the strain data to negligible levels. The power mains lines are also reduced to about 10% of their original power, as shown in Figs. 2 and 4. The overall change to the amplitude spectral density (ASD) is shown in Fig. 5. Additional cleaning of the power mains lines is performed by a separate algorithm [6].

IV. CONCLUSION

The removal of narrow-band features in LIGO strain data was successfully implemented in O3. All but the sub-10 Hz and roaming calibration lines were removed with very high quality with minimal remaining residual. The 60 Hz power mains line and the 120 Hz and 180 Hz harmonics of this line were reduced by nearly 90% in the L1 detector and close to 100% in the H1 detector. The success of the removal of the power mains lines does vary somewhat across the observing run, but the results presented here are an accurate representation of the average results obtained from the subtraction methods outlined in this paper.

In future observing runs, we will continue to subtract calibration lines and power mains lines and hope to additionally include broadband noise subtraction when possible. The software needed for broadband noise subtraction has already been developed in the `gstlal-calibration` software package, but it requires a reliable witness channel for the broadband noise source. We hope to streamline the additional cleaning of the power mains lines sidebands currently done using the algorithm outlined in [6]. It is our eventual goal to provide all of the above in low latency as well as in high latency.

[1] D. Davis and et al., arXiv e-prints , arXiv:2101.11673 (2021), arXiv:2101.11673 [astro-ph.IM].

[2] S. Karki, D. Tuyenbayev, S. Kandhasamy, B. P. Abbott, T. D. Abbott, E. H. Anders, J. Berliner, J. Betzwieser, C. Cahillane, L. Canete, C. Conley, H. P. Daveloza, N. De Lillo, J. R. Gleason, E. Goetz, K. Izumi, J. S. Kissel, G. Mendell, V. Quetschke, M. Rodruck, S. Sachdev, T. Sadecki, P. B. Schwinberg, A. Sottile, M. Wade, A. J. Weinstein, M. West, and R. L. Savage, Review of Scientific Instruments **87**, 114503 (2016), https://doi.org/10.1063/1.4967303.

[3] N. A. Robertson, G. Cagnoli, D. R. M. Crooks, E. Elliffe, J. E. Faller, P. Fritschel, S. Go$szlig$ler, A. Grant, A. Heptonstall, J. Hough, H. L$uuml$ck, R. Mittleman, M. Perreur-Lloyd, M. V. Plissi, S. Rowan, D. H. Shoemaker, P. H. Sneddon, K. A. Strain, C. I. Torrie, H. Ward, and P. Willems, Classical and Quantum Gravity **19**, 4043 (2002).

[4] S. M. Aston, M. A. Barton, A. S. Bell, N. Beveridge, B. Bland, A. J. Brummitt, G. Cagnoli, C. A. Cantley, L. Carbone, A. V. Cumming, L. Cunningham, R. M. Cutler, R. J. S. Greenhalgh, G. D. Hammond, K. Haughian, T. M. Hayler, A. Heptonstall, J. Heefner, D. Hoyland, J. Hough, R. Jones, J. S. Kissel, R. Kumar, N. A. Lockerbie, D. Lodhia, I. W. Martin, P. G. Murray, J. O'Dell, M. V. Plissi, S. Reid, J. Romie, N. A. Robertson, S. Rowan, B. Shapiro, C. C. Speake, K. A. Strain, K. V. Tokmakov, C. Torrie, A. A. van Veggel, A. Vecchio, and I. Wilmut, Classical and Quantum Gravity **29**, 235004 (2012).

[5] "GstLAL documentation," https://lscsoft.docs.ligo.org/gstlal/.

[6] G. Vajente, Y. Huang, M. Isi, J. C. Driggers, J. S. Kissel, M. J. Szczepańczyk, and S. Vitale, Phys. Rev. D **101**, 042003 (2020).

[7] Virgo Collaboration, arXiv e-prints , arXiv:1807.03275 (2018), arXiv:1807.03275 [gr-qc].

[8] D. Tuyenbayev, S. Karki, J. Betzwieser, C. Cahillane, E. Goetz, K. Izumi, S. Kandhasamy, J. S. Kissel, G. Mendell, M. Wade, A. J. Weinstein, and R. L. Savage, Classical and Quantum Gravity **34**, 015002 (2016).

[9] A. D. Viets, M. Wade, A. L. Urban, S. Kandhasamy, J. Betzwieser, D. A. Brown, J. Burguet-Castell, C. Cahillane, E. Goetz, K. Izumi, S. Karki, J. S. Kissel, G. Mendell, R. L. Savage, X. Siemens, D. Tuyenbayev, and A. J. Weinstein, Classical and Quantum Gravity **35**, 095015 (2018).

Line	Purpose	L1 frequency (Hz)	H1 frequency (Hz)	Subtracted?
$f_4^{(pc)}$	SRC detuning	n/a	7.93	No
f_{U}	κ_{U}	15.1	15.6	Yes
f_{P}	κ_{P}	15.7	16.4	Yes
$f_1^{(pc)}$	κ_{T}, κ_{P}, κ_{U}	16.3	17.1	Yes
f_{T}	κ_{T}	16.9	17.6	Yes
$f_2^{(pc)}$	κ_{C}, f_{cc}	434.9	410.3	Yes
$f_3^{(pc)}$)	high-frequency check	1083.1	1083.7	Yes
$f_5^{(pc)}$	high-frequency check	roaming	roaming	No

TABLE I: This table outlines the calibration line frequencies present in the LIGO Hanford (H1) detector and LIGO Livingston (L1) detector during O3. A superscript of (pc) indicates that the line frequency corresponds to a photon calibrator injection. The table also indicates the purpose the lines and whether each line was subtracted from the strain data. Many of these calibration lines are used in calculating time-dependent parameters for the calibration model, such as κ_{U}, κ_{P}, κ_{T}, κ_{C}, f_{cc}, and the signal recycling cavity (SRC) detuning parameters f_s and Q^{-1} [8, 9].

Channel Name	Purpose
CAL-PCALY_RX_PD_OUT_DQ	Subtracting all photon calibrator lines ($f_{(1-4)}^{(pc)}$)
SUS-ETMX_L3_CAL_LINE_OUT_DQ	Subtracting the TST/L3/ESD line (f_{T})
SUS-ETMX_L2_CAL_LINE_OUT_DQ	Subtracting the PUM/L2 line (f_{P})
SUS-ETMX_L1_CAL_LINE_OUT_DQ	Subtracting the UIM/L1 line (f_{U})
PEM-EY_MAINSMON_EBAY_1_DQ	Subtracting the power mains lines

TABLE II: Witness channels used for subtracting each of the line features from the LIGO strain data.

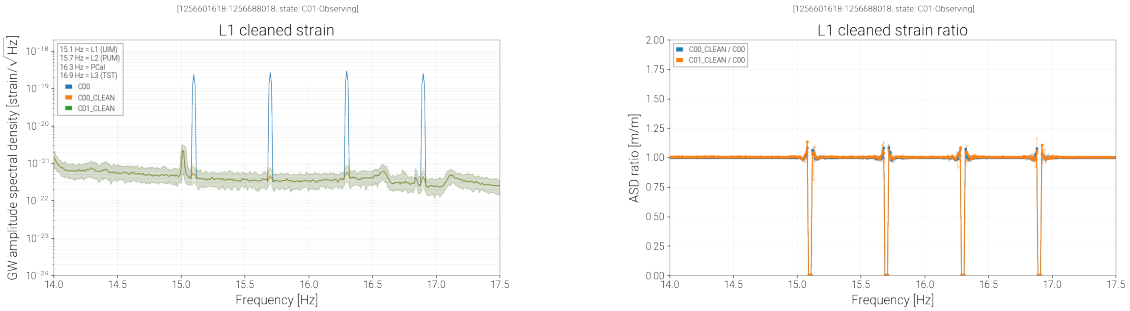

FIG. 1: (Left) Comparison of the cleaned L1 strain data from the low-latency calibration (C00_CLEAN) and the high-latency calibration (C01_CLEAN) to the low-latency strain data without any lines subtracted (C00) at the low-frequency calibration lines. (Right) Ratio of the cleaned L1 strain data from the low-latency calibration and the high-latency calibration to the low-latency strain data without any lines subtracted at the low-frequency calibration lines.

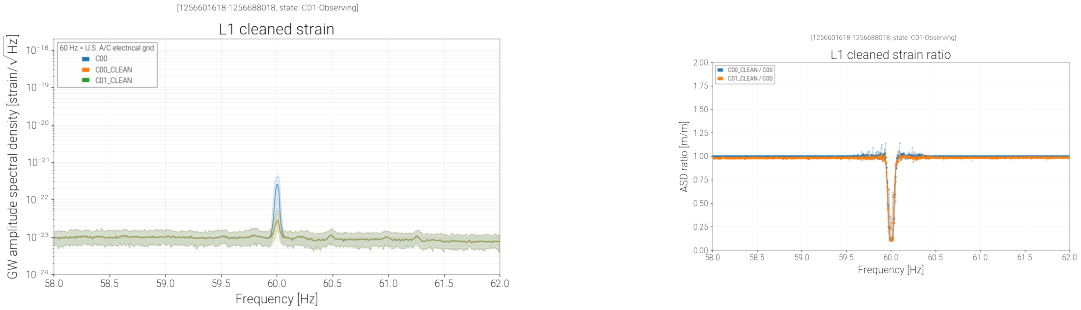

FIG. 2: (Left) Comparison of the cleaned L1 strain data from the low-latency calibration (C00_CLEAN) and the high-latency calibration (C01_CLEAN) to the low-latency strain data without any lines subtracted (C00) at the 60 Hz power mains line. (Right) Ratio of the cleaned L1 strain data from the low-latency calibration and the high-latency calibration to the low-latency strain data without any lines subtracted at the 60 Hz power mains lines.

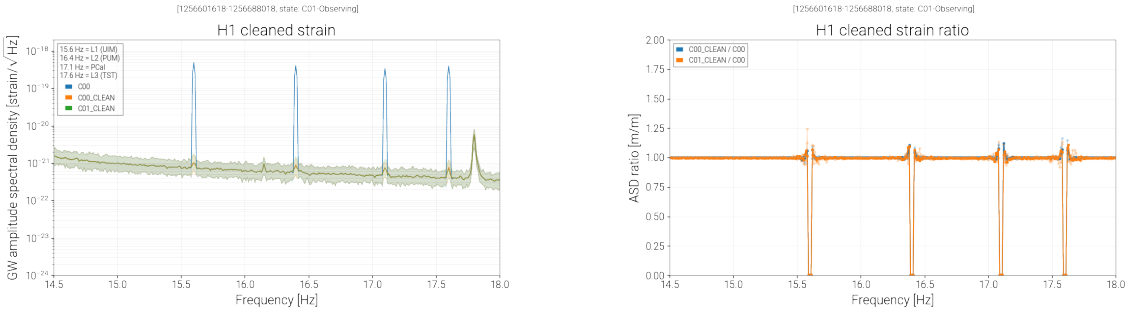

FIG. 3: (Left) Comparison of the cleaned H1 strain data from the low-latency calibration (C00_CLEAN) and the high-latency calibration (C01_CLEAN) to the low-latency strain data without any lines subtracted (C00) at the low-frequency calibration lines. (Right) Ratio of the cleaned H1 strain data from the low-latency calibration and the high-latency calibration to the low-latency strain data without any lines subtracted at the low-frequency calibration lines.

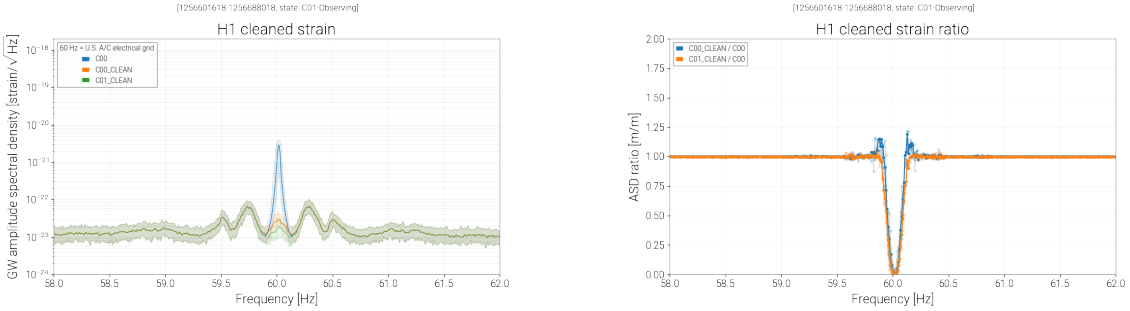

FIG. 4: (Left) Comparison of the cleaned H1 strain data from the low-latency calibration (C00_CLEAN) and the high-latency calibration (C01_CLEAN) to the low-latency strain data without any lines subtracted (C00) at the 60 Hz power mains line. (Right) Ratio of the cleaned H1 strain data from the low-latency calibration and the high-latency calibration to the low-latency strain data without any lines subtracted at the 60 Hz power mains line.

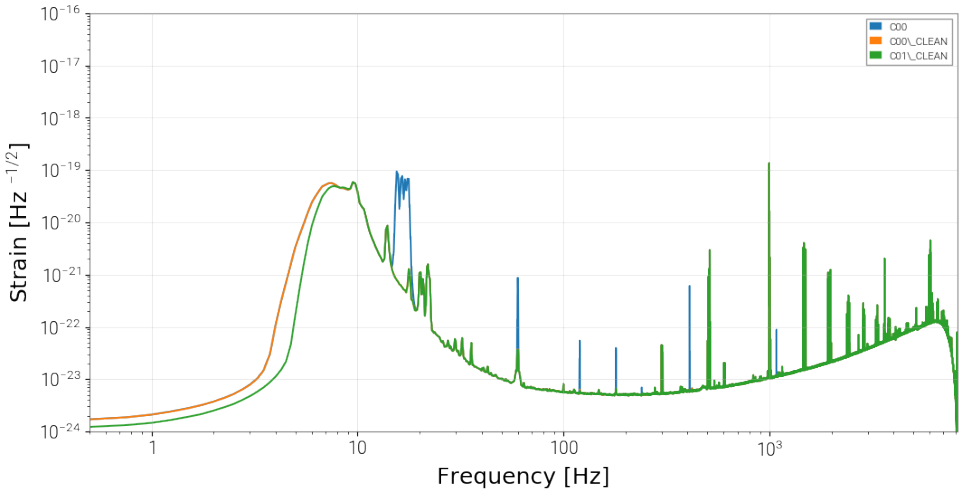

FIG. 5: Amplitude spectral density (ASD) comparison for H1 between the low-latency strain data with no cleaning applied (C00), the low-latency strain data with calibration lines and power mains lines removed (C00_CLEAN), and the high-latency strain data with calibration lines and power mains lines removed (C01_CLEAN).